Design and Operation of ETA, an Automated Ellipsometer

Abstract: The design and operational features are described for a computer-assisted ellipsometer (called ETA for Ellipsometric Thickness Analyzer), developed to provide reliable, real-time measurement of field-effect transistor gate insulator thickness in a manufacturing environment. ETA illuminates the sample with light of fixed polarization and uses a rotating analyzer to measure the polarization of the reflected light. Sample alignment is done automatically by ETA, so that usually no operator adjustments are required. Fourier analysis of the light transmitted by the analyzer is used to reduce noise and enhance measurement precision.

In its normal mode of operation (incident light linearly polarized at 45°), ETA can measure single and double-layer films of SiO₂ and Si₃N₄ in the thickness range of 300 to 800 Å with precision comparable to that of conventional ellipsometers. Other modes of operation, which make use of a fixed-position compensator in the incident light path, allow precise measurement of thin films (0 to 300 Å) and permit use of ETA as a general-purpose ellipsometer. The typical time interval required for wafer alignment, data acquisition, analysis and recorded output of film thickness is about five seconds, and the measurement reproducibility is typically about 1 Å.

Introduction

Optical methods for measuring the thickness of transparent films are widely used in the semiconductor industry. These methods have the attractive features of being both precise and nondestructive, the precision resulting from the similarity in magnitude of the wavelength of the light and the film thickness. The techniques may generally be classified as being either photometric or polarimetric, depending on whether the basic information is carried by the intensity or the polarization state of the detected light. In the first instance, some interference mechanism is usually involved, whereby one essentially counts the number of wavelengths that fit inside the film. Examples are CARIS [1], where reflectance is measured at a fixed angle of incidence (usually near normal) as the wavelength is varied, and VAMFO [2], which measures reflectance at a fixed wavelength as the angle of incidence is varied. Interference techniques are generally limited to films of optical thicknesses greater than a quarter of a wavelength. Ellipsometry is a polarimetric technique that has undergone a great deal of development and refinement over the last ten years [3]. With this technique, the change in polarization state of light caused by reflection from a film-covered surface is measured at a fixed angle of incidence.

The unique feature of ellipsometry is that this change in polarization is a strong function of thickness, even for extremely thin films. In addition, the refractive index of the film is obtained so long as its optical thickness is greater than about $\lambda/20$. Another application of ellipsometry is the measurement of individual layer thicknesses of double-layer films, when the refractive indices differ sufficiently and are known (e.g., Si_3N_4 -SiO₂ films on silicon). These considerations have taken on significance recently in the semiconductor industry with the use of thin-film and double-layer gate insulators in field-effect transistor (FET) technology, and ellipsometry has consequently become a measurement tool of substantial importance.

As commonly practiced, however, ellipsometry is a tedious and time-consuming measurement, and the skill required on the part of the operator to extract the precision available in the technique places it almost in the category of an art. Five minutes or more may be consumed in carefully aligning the sample on its holder, finding polarizer and analyzer settings for nulls in two ellipsometric "zones" (which are necessary to cancel the effect of imperfections present in most compensators), averaging the readings, and calculating the ellipsometric sample parameters ψ and Δ . These must be analyzed subsequently by means of tables, graphs, or a computer to obtain film thickness.

It is clear that, particularly in a manufacturing environment, the value of a measurement diminishes rapidly with the time one must wait for the final result, i.e., the determined film thickness. Conversely, the value of the measurement would increase substantially if it could be

made fast enough to permit changing from an off-line, test-wafer mode to an on-line measurement of every product wafer. In that case, not only could "out-of-spec" wafers be removed (eliminating the wasted expense of further processing), but also parameter drifts could be detected and corrected in time to keep the process within specification. In the case of ellipsometry, automation would also remove the dependence of measurement quality on operator skills.

Ellipsometry has been automated to varying degrees using a number of methods by other workers. Most of these techniques employ the conventional ellipsometric approach whereby a null in detected light intensity is obtained, using in some instances stepping motors instead of the operator's hands. In other cases, Faraday cells, producing continuous modulation of the polarization of the incident and reflected light, are used along with phase-sensitive detection techniques. Angular resolution obtained is typically as good or better than that characteristic of manual operation (0.01°). The main achievement of these techniques is a greatly reduced measurement time interval. This is usually on the order of one second, but in the case of an ellipsometer described by Cahan and Spanier [3], measurements are made at a rate of 50 per second. Their approach was to use a continuously rotating analyzer in the reflected light path (as is done in the present case) and obtain a measurement of polarization for each rotation of the analyzer. Importantly, developments such as these permit ellipsometric investigations of rapidly changing systems, such as the dynamics of film growth, which were previously impossible. The interested reader is referred to the papers contained in the two international symposiums on ellipsometry (particularly the later one) given in Ref. 3 for more information on automation techniques, as well as for additional references to papers dealing with many other aspects of ellipsometry.

In terms of bringing automated ellipsometry to the semiconductor manufacturing environment, as described above, there are two essential capabilities that are absent from existing systems, namely, automatic sample alignment and immediate data analysis to determine film thickness and to allow decisions based on the measurements to be made in real time. These two areas have been largely, if not totally, excluded from automation efforts, which are directed mainly toward the rapid and precise acquisition of polarimetric data. Our purpose in developing an automated ellipsometer, then, was to address the *entire* measurement process, from sample placement to film thickness determination, to produce a high measurement "throughput" capability and as nearly an "operatorless" environment as possible.

Specific design constraints included the use of a small, dedicated computer (such as IBM 1130, IBM System/7,

etc.), but not in a mode where it would attempt to simulate a human operator on an otherwise conventional instrument. In the anticipation that most measurements would be made on silicon wafers, some normal instrument variables were fixed, e.g., the angle of incidence (70°) and the height of the sample stage. Wafer alignment was thus reduced to rotations about two axes, and this was to be automated. To allow for automatic wafer loading and positioning, front and back clearances were maintained at sample height, and space was provided for a stepping-motor-driven x-y table. The instrument was to give film thickness and refractive index (not just ψ and Δ) within a maximum of ten seconds. Operator adjustments were to be minimized or eliminated. The "rotating analyzer" technique was selected as being particularly well suited to automated measurement, because it requires sampled data taken as a function of position of a single optical component. Manual ellipsometry involves the positioning of two optical components to produce a null - a task performed well by human beings but not nearly so well by computers. On the other hand, computers can take quantitative data very rapidly and do lengthy calculations with ease. With the computer as an integral part of the instrument, the result is available within a framework where it can be the basis for taking immediate action, if necessary. This design approach parallels that of a previously developed automated spectrophotometer [4], of which the measurable thickness range is complemented by the present instrument.

This paper describes the design and operation of the new ellipsometer, which is called ETA (Ellipsometric Thickness Analyzer).

Overall system description

Figure 1 is an overall representation of ETA that shows the flow of information and identifies parameters defined later in the text. ETA can be regarded as a system that comprises three interconnected parts. The first is basically optical and mechanical, and is similar to a conventional ellipsometer. Monochromatic light passes through fixed polarizing components, reflects from the automatically aligned sample and passes through a rotating analyzer, emerging as a beam with cyclically varying intensity. The second part of the system is electrical. It detects, samples and digitizes the emerging light intensity at discrete angular positions of the analyzer and passes this information on to the third part of the system, which consists of the computer and a set of control and analysis programs. Here the data for intensity versus analyzer azimuth are analyzed to obtain the polarization state of the reflected light. Knowledge of the polarization of the incident light gives the change in polarization caused by the reflection. Numerical ellipsometric analysis then gives the film thickness and refractive index.

473

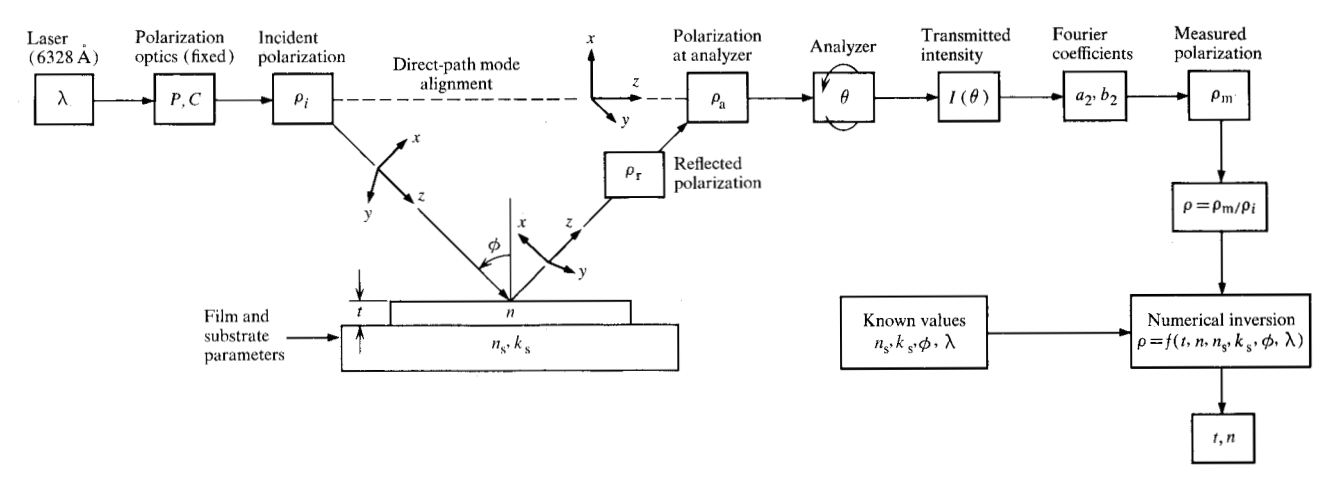


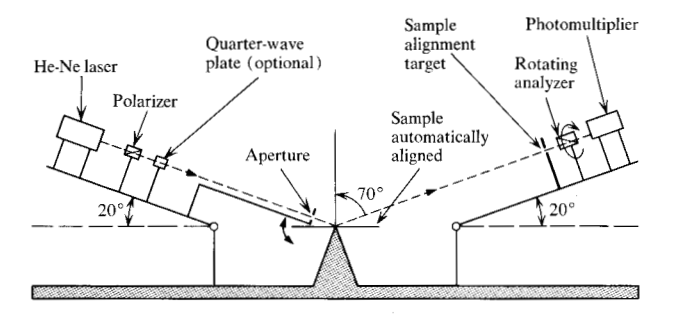
Figure 1 Functional and pictorial representation of ETA.

Optical and mechanical components

Figure 2 shows in more detail the major components of the optical-mechanical section of ETA. The light source is a 1-mW He-Ne laser that provides a sufficiently intense, collimated beam of 6328-Å radiation without use of collimating optics. A polarized laser is used to eliminate intensity variations arising from switching between polarization modes. The laser has a well-regulated power supply and is housed in a cylinder that is coaxial with the light beam. The head is mounted on a veeblock, which allows its removal and replacement without the necessity of realigning the optical system.

To eliminate the need to have an operator make precise azimuth settings of adjustable optical components, as with conventional ellipsometers, ETA keeps component adjustment to a minimum and uses pinned-position component mounts. These are shown in Fig. 3(b). The polarizer can be set and pinned at three positions with 0.02° repeatability, while the compensator, if used, is locked at a single position and simply inserted or removed from the light path. Normal operation is with the compensator removed and the polarizer set at 45° to the

Figure 2 Optical and mechanical components of ETA.



plane of incidence. A 0° polarizer setting is provided for initial system alignment, and an alternative measurement position of 12° is used when the compensator (set with the fast axis at 90°) is inserted. As will be explained later, the alternative setting provides increased sensitivity for measuring films thinner than $300 \,\text{Å}$.

A limiting aperture (typically 0.25 mm in diameter) placed near the sample determines the size of the area measured. After reflection from the sample, the light beam passes through a control aperture, located about 0.5 m from the point of reflection, and the rotating analyzer, which is driven at a constant speed of 300 rpm by a small ac synchronous motor. The beam then passes through a diffuser and fiber optic bundles to a photomultiplier tube (PMT), which is used as a linear detector. The laser-PMT combination provides sufficient sensitivity to compensate for light lost in the diffuser and input aperture. The diffuser and fiber optic bundles serve to depolarize the light coming from the analyzer and thus eliminate any effects due to polarization-dependent sensitivity of the detector. They also reduce spurious effects caused by residual beam deflection when the light passes through the analyzer, and they allow convenient placement of the PMT.

The components of the optical system are mounted on arms that can be set for a 70° fixed angle of incidence or lowered to a horizontal position to allow system alignment in a direct-path mode. The condition of fixed angle of incidence allows the use of two separate pivots about 0.5 m apart for the input and output arms, providing space in the vicinity of the sample for the automatic alignment mechanism, which is described below. For the direct-path mode, the sample lies below the light path, so that it does not interfere with operation in that mode. A photograph of the entire instrument is shown in Fig. 3 (a).

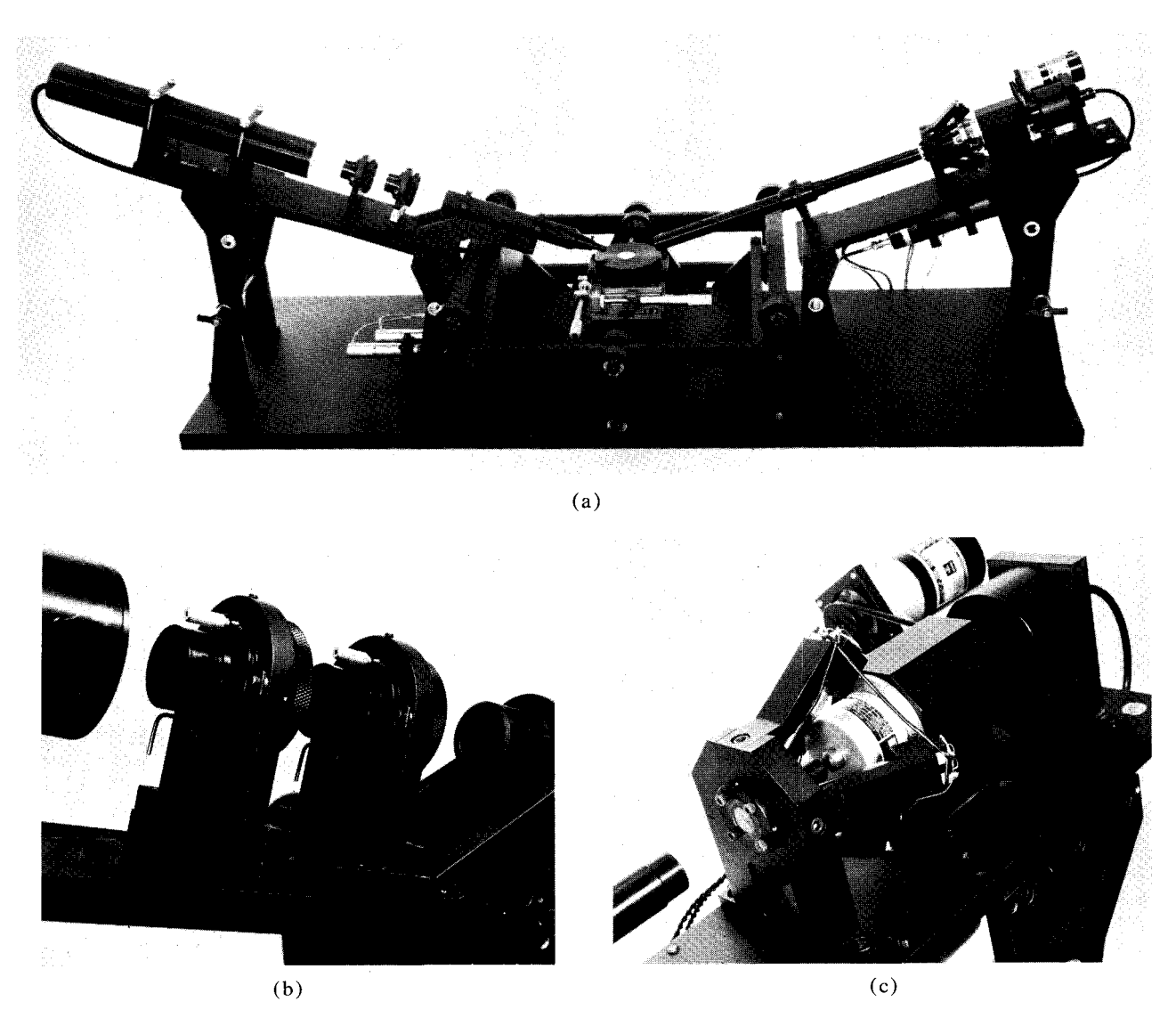
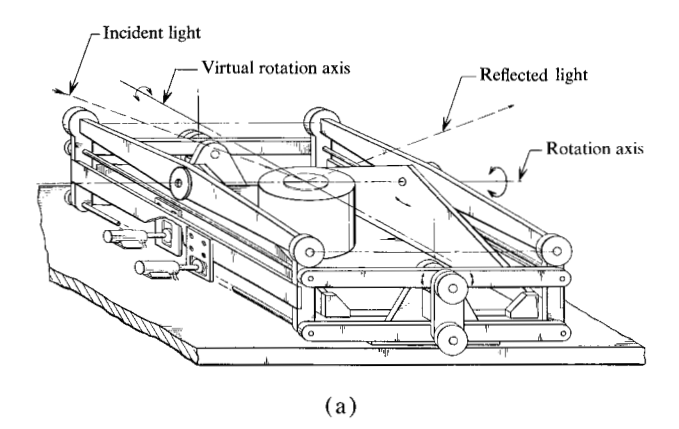


Figure 3 Photographs of ETA showing (a) the entire instrument, (b) the pinned-position polarizer and compensator mounts in the incident light path, and (c) the control aperture.

Automatic sample alignment is included to eliminate an important operator adjustment. Alignment is simplified for the measurement of semiconductor wafers because wafer thicknesses are sufficiently constant that the stage can be set and fixed at the proper height without requiring subsequent adjustment. Sample alignment is then accomplished by tilting the stage about two perpendicular axes which intersect on the surface of the sample at the point of reflection. This arrangement insures that, once the sample is positioned as desired, the measurement location is not moved by the alignment procedure. A cradle mechanism shown in Fig. 4(a) is used to hold the stage and sample and is hung from a real pivot in the plane of the measurement at the sample height. It is large enough to accommodate a commercially available,

stepping-motor-driven x-y table having 5-cm travel (not shown on Fig. 4), so that the measurements at a number of precise locations on a single wafer can be efficiently made. Normal to the plane of measurement, a parallelogram arrangement provides a virtual pivot at sample height with no interference for wafer loading and unloading. Drives for motion on these two axes are provided by cam assemblies driven by two small dc servomotors, producing a total angular travel of about 1°. The control aperture shown in Fig. 4(b) serves as a reflected-beam deviation detector and actuates the servos to tilt the sample stage so as to direct the reflected beam through the center of the aperture. To accomplish this, the control aperture is surrounded by four fiber optic bundles, each covering one quadrant sector



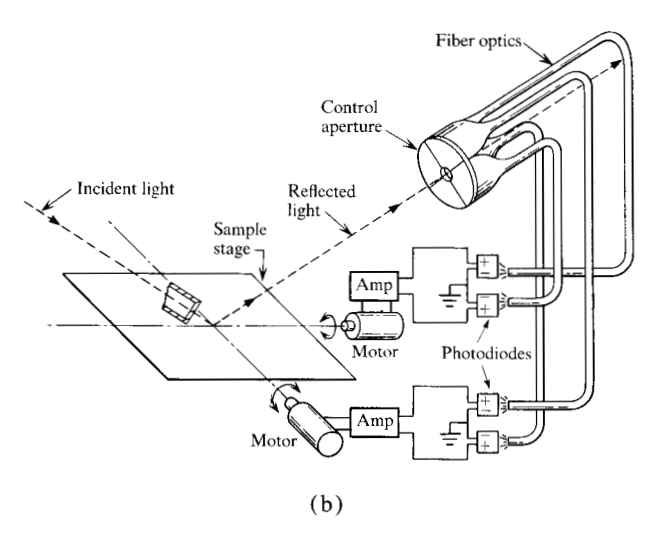


Figure 4 The automatic sample alignment system. (a) The sample-leveling mechanism, showing the virtual axis that provides front and rear clearances to permit automatic wafer loading. Motors driving cams in slots provide motion for leveling on two rotation axes that intersect at the point of reflection. (b) Pictorial representation of the control aperture with its fiber optics. The control aperture actuates the servomotors.

and terminated with a silicon photodetector. These are connected pairwise to operational amplifiers that drive the two servos. Sample alignment time is typically one-half second and repeatability is on the order of 0.01° . A photograph of the control aperture is shown in Fig. 3(c).

Data acquisition

The scheme for the electrical interface to the computer is shown in Fig. 5. The angular position of the spinning analyzer is sensed by an incremental optical encoder mounted on a common hollow shaft. The encoder has two ouputs, one which gives a single "start" pulse per rotation to synchronize the system, and another which gives pulses at equally spaced angular intervals, 256 per rotation. The output of the PMT is amplified by an operational amplifier, not shown in Fig. 5, and fed to an ana-

log-to-digital converter (A/D). The A/D begins conversion when triggered by the pulses from the optical encoder and signals the computer to read its output when the conversion is completed. A measurement thus proceeds as follows: A sample is placed on the stage and is automatically aligned. A signal from the operator (e.g., generated by pressing a button) causes the computer to go into a "wait" state until the start pulse is detected. The computer then enables recognition of the conversion-complete pulse from the A/D, so that data can be acquired. Data are taken either for a single rotation of the analyzer or for several rotations and are averaged to further suppress noise. When the appropriate number of data points (256 times the number of rotations) has been read, the computer disables recognition of the conversion-complete pulse and data acquisition ceases.

The analyzer rotates with a constant speed of 300 rpm so that the data acquisition rate is 1280 per second. The conversion time of the A/D is about ten microseconds, during which time the analyzer rotates less than 0.02°, so that the readings of the light intensity are almost instantaneous.

The data read by the computer are thus proportional to the intensity of the light transmitted by the analyzer, sampled at 256 equally spaced angular positions, covering one complete rotation. The angle, relative to the plane of incidence, of the first reading following the start pulse is determined by an initial alignment, which is described later.

Data analysis

Figure 6 indicates the method of analyzing the intensity data. A Fourier analysis reduces the digital data to two parameters that relate to the polarization state of the measured light. From these the ellipsometric sample parameters ψ and Δ are determined. Ellipsometric analysis then determines the film thickness and refractive index.

• Fourier analysis

The first step in the analysis of the digital intensity data is a Fourier analysis to reduce the data to two parameters which relate to the polarization state of the measured light. This step makes use of the fact that, for light of any polarization incident on the rotating analyzer, the intensity of the transmitted light has the form

$$I(\theta) = I_0(1 + a_2 \cos 2\theta + b_2 \sin 2\theta), \tag{1}$$

where θ is the azimuth of the transmitting axis of the analyzer, measured counterclockwise from the plane of incidence looking toward the source, and I_0 is the average intensity for a full rotation of the analyzer. The coefficients a_2 and b_2 represent all the polarization information that is available from the measurement [5]. They are

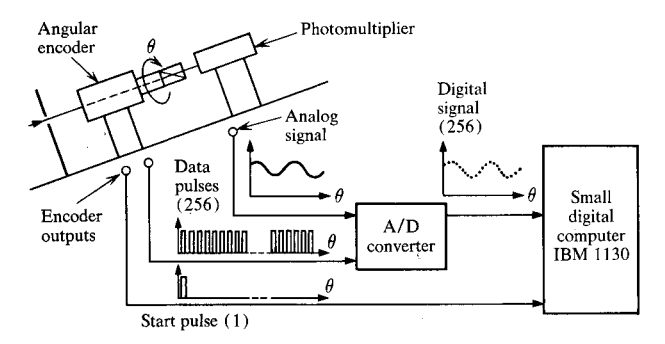


Figure 5 Electrical components of ETA.

determined by numerical evaluation of the coefficients of the discrete Fourier series, as described by Budde[6], or other equivalent means such as fast Fourier transform algorithms.

All harmonics present in the data, other than the zeroth and second, arise from random measurement noise or nonideal operation of the instrument. They may be evaluated and used as a check that the system is performing as expected. Any harmonic that is present with magnitude greater than 0.005, relative to an average value of unity, is treated as significant and is suggestive of a particular departure from ideal system behavior. For example, a first-harmonic variation can arise if the analyzer deflects the direction of the transmitted light, and it may indicate that the fiber optic bundle is placed too close to the diffusing plate. Fourth-harmonic variation can be produced by nonlinear response or saturation of the PMT, the signal operational amplifier, or the A/D, and may indicate that there is too much light or that the PMT supply voltage is set too high. Random appearance of other harmonics can arise because of improper triggering of the A/D, resulting either in missing data or in the presence of spurious data. Thus there is a convenient means by which proper system performance can be verified independently of the polarization measurement. This is of great value, particularly during initial optical alignment and electrical checkout of the system.

• Polarization of measured light

The polarization state of polarized light has several common parametric representations. One that is useful for system alignment is azimuth α and ellipticity tan χ (ratio of minor to major axis) of the electric field polarization ellipse. Some authors add as a third parameter the rotational sense in which the ellipse is generated, called the left or right "handedness" of the polarization. However, this may simply be incorporated in a consistent manner into the numerical sign of χ : positive

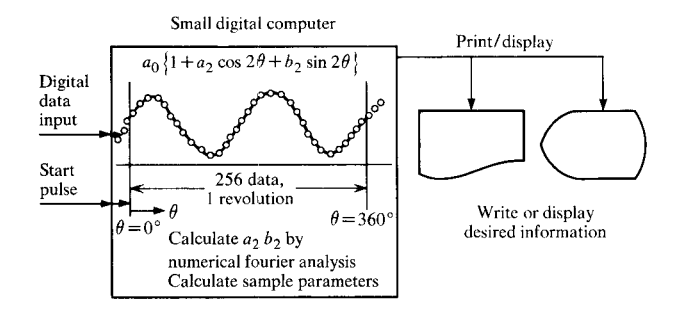


Figure 6 Pictorial representation of the data analysis, illustrating the form of the acquired intensity data and the Fourier reduction to two parameters.

for right-handed and negative for left-handed polarization. The ranges of values necessary to describe all polarization states are $-90^{\circ} < \alpha \le 90^{\circ}$ and $-45^{\circ} \le \chi \le 45^{\circ}$. The Fourier coefficients in (1) for a measurement of polarized light described by (α, χ) (see Appendix 1) are

$$a_2 = \cos 2\chi \cos 2\alpha, \tag{2}$$

$$b_2 = \cos 2\chi \sin 2\alpha. \tag{3}$$

Inspection of Eqs. (2) and (3) shows that the coefficients a_2 and b_2 describe the polarization completely except for the sign of χ , which is indeterminate because the cosine is an even function.

A polarization description applicable to ellipsometric analysis is the relative magnitude and phase of the electric field components along two orthogonal axes. It is customary for the axes to be right-handed Cartesian coordinates with the z-axis along the direction of light propagation, the x-axis in the plane of incidence, and the y-axis in the plane of the sample, as indicated in Fig. 1. Letting tan ψ_a be the x-to-y amplitude ratio and Δ_a be the x-to-y relative phase, all polarization states are described for $0^{\circ} \leq \psi_a \leq 90^{\circ}$ and $0^{\circ} \leq \Delta_a < 360^{\circ}$. (The subscript "a," when used in this paper, denotes light falling on the analyzer.) The Fourier coefficients for a measurement of polarized light described by (ψ_a, Δ_a) are, as discussed in Appendix 1,

$$a_2 = -\cos 2\psi_a,\tag{4}$$

$$b_{a} = \sin 2 \,\psi_{a} \cos \Delta_{a}. \tag{5}$$

Inspection of (4) and (5) again shows that the coefficients describe the polarization completely except for the handedness, which is indeterminate because Δ_a may be more or less than 180° by equal amounts without affecting the value of b_2 . Inverting (4) and (5) (as in Appendix 1) gives measured values (ψ_m, Δ_m) in terms of the Fourier coefficients, from which is obtained: $\psi_a = \psi_m$ and $\Delta_a = \Delta_m$ or $360^\circ - \Delta_m$.

477

• Determination of ψ and Δ

To describe this part of the analysis, it is convenient to introduce the complex parameter ρ_a to represent the polarization

$$\rho_{\mathbf{a}} = \tan \,\psi_{\mathbf{a}} \,e^{i\Delta_{\mathbf{a}}}. \tag{6}$$

This is the ratio of the complex amplitudes of the electric field components along the x and y directions at the analyzer. The polarization of the light incident and reflected from the sample is described respectively by the parameters ρ_i and ρ_r defined as in (6) by their representations (ψ_i, Δ_i) and (ψ_r, Δ_r) . Thus, when the arms of the ellipsometer are lowered to the direct-path mode, the incident light is measured $(\rho_a = \rho_i)$, and in the usual 70° measurement mode the reflected light is measured $(\rho_a = \rho_r)$. The object of ellipsometry is to determine the complex ratio ρ of the reflected and incident polarization state parameters, represented by (ψ, Δ) :

$$\rho = \rho_{\rm r}/\rho_{\rm i} = \tan \psi \, e^{i\Delta}. \tag{7}$$

This is determined with ETA (Fig. 1) by providing incident light with a known polarization ρ_i , measuring the reflected light polarization ($\rho_a = \rho_r$) and taking the ratio as indicated in (7).

The selection of a particular incident polarization state ρ_1 defines a mode of operation for ETA. The incident polarization may be adjusted by the angular positions, or azimuths, of the polarizer and of the compensator, if present in the incident light path. For all the situations described in this paper, the compensator remains fixed in its holder with the fast axis set at 90° to the plane of incidence (the x-axis), so that the only adjustment required is its insertion or removal from the light path.

The simplest input configuration has the compensator absent and the polarizer set at 45°. This gives equal amounts of x- and y-oriented light ($\psi_i = 45^\circ$) which are in phase with each other ($\Delta_i = 0^\circ$). Thus, $\rho_i = 1$ and, according to (7), $\rho = \rho_a$. That is,

$$\psi = \psi_{\rm a}, \qquad \Delta = \Delta_{\rm a}.$$
 (8)

This is the usual mode of operation for ETA, and will be referred to as the *normal* measurement mode.

An alternate input configuration is particularly useful for measuring very thin (<300 Å) films on silicon. Here the compensator is inserted at 90° and the polarizer is moved to its alternate pinned position of 12°. The effect of this set of azimuth values is to make light reflected from bare silicon to be nearly circularly polarized, with the polarization gradually changing to a linear state as the thickness of a film on the silicon increases. The optical behavior of the compensator is characterized by the complex ratio of the transmission coefficients along its slow and fast axes, given by

$$T_{\text{slow}}/T_{\text{fast}} = \tan \psi_{\text{c}} e^{-i\Delta_{\text{c}}}.$$
 (9)

The incident polarization for this mode of operation is

$$\rho_{\rm i} = \cot (12^{\circ}) \tan \psi_{\rm c} e^{-i\Delta_{\rm c}} \tag{10}$$

so that, from (7),

$$\tan \psi = \tan \psi_a \tan (12^\circ) \cot \psi_c,
\Delta = \Delta_a + \Delta_c.$$
(11)

This configuration will be referred to as the *thin-film* measurement mode.

For an ideal compensator, $\psi_c=45^\circ$ and $\Delta_c=90^\circ$. In practice, however, these quantities differ from their ideal values, and must be determined experimentally for the compensator to be correctly used. ETA allows an extremely simple and straightforward measurement of ψ_c and Δ_c when used in the direct-path mode, as is seen from (11). In this mode (setting tan $\psi=1$ and $\Delta=0$) we have

$$\tan \psi_c = \tan \psi_a \tan P, \qquad \Delta_c = -\Delta_a, \qquad (12)$$

where P is the azimuth of the polarizer. One sees from this that, for any polarizer setting, Δ_c is given by the magnitude of Δ_a directly, and if P is set to 45° , ψ_c is simply given by ψ_a . This measurement need be performed only once to characterize the compensator. Then when ETA is used with the compensator for thickness measurement, the measured values of ψ_a and Δ_a are used in (11) with ψ_c , Δ_c and the 12° polarizer setting to determine ψ and Δ . A single measurement, with ψ_c and Δ_c taken explicitly into account, thus replaces the averaged results of two measurements in complementary ellipsometric zones [7] usually performed in manual ellipsometry.

• Determination of sample parameters

The final step in the analysis is the determination of film thickness t and refractive index n from the experimentally determined values of ψ and Δ . The relationship of these parameters depends on the wavelength λ , the angle of incidence ϕ , and the complex substrate refractive index $\hat{n}_s = n_s - ik_s$. The equations describing this relationship can be found in the literature in most papers on ellipsometry [7]. It is sufficient for our purposes to state that for transparent films the relationship takes the form

$$\rho = \tan \psi \, e^{i\Delta} = f(t, n, n_s, k_s, \phi, \lambda), \tag{13}$$

where f represents a complex transcendental function which cannot be solved explicitly for t and n. Graphs showing lines of constant film thickness or refractive index can be made for a set of $(n_s, k_s, \phi, \lambda)$ values to show the relationship of n and t to ψ and Δ , and to obtain

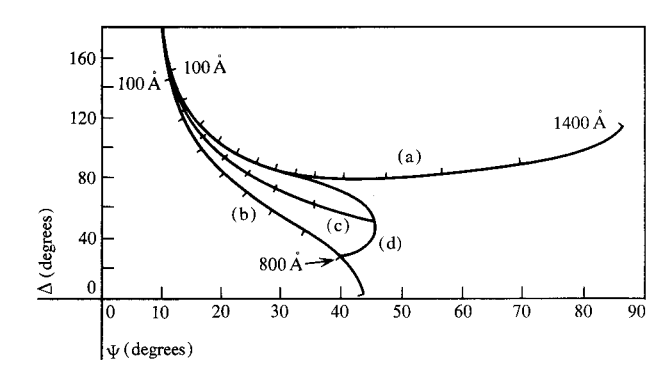


Figure 7 Graph of the parameters ψ and Δ for films on silicon. Parameters used are $n_{\rm S}=3.855,\ k_{\rm S}=0.024,\ \phi=70^\circ$ and $\lambda=6328$ Å. The curves represent (a) SiO₂ film (n=1.457) of thickness 0 to 1400 Å, (b) Si₃N₄ film (n=1.98) of thickness 0 to 900 Å, (c) Si₃N₄-SiO₂ double-layer film with equal layer thicknesses and total film thickness 0 to 800 Å, and (d) double-layer film of varying layer thicknesses, keeping the total film thickness at 800 Å. Curves (a) to (c) are marked in 100-Å steps.

approximate answers. Figure 7 shows a graph of this type for $n_s = 3.855$, $k_s = 0.024$, $\phi = 70^{\circ}$ and $\lambda = 6328$ Å which applies to ETA for measurement of films on silicon wafers [8]. Curves (a) and (b) are lines of constant refractive index, corresponding respectively to SiO, (n = 1.457) for t = 0 to 1400 Å and Si₂N₄ (n = 1.98) for t = 0 to 900 Å, marked in 100-Å steps. ETA provides a numerical inversion of (13) by supplying initial estimates of t and n, calculating ψ and Δ values from (13) and comparing them with the measured values. The estimates are successively improved, using a Newton-Raphson iteration technique, until calculated and measured values agree to within 0.01° . The values of t and n which give this agreement are then taken as correct. Although the refractive index of a film is usually known, the thickness may be completely unknown. Since with poor intial estimates the iteration procedure may not converge to an answer, ETA is programmed to calculate an initial thickness estimate from ψ and Δ and the nominal film refractive index. This is possible because (13) may be solved analytically for t, by itself, in terms of all the other parameters [7]. Using the calculated initial guess for thickness and the nominal film refractive index as a starting point, the iteration routine usually converges to an answer in three or four tries. A flow chart of this procedure is shown in Fig. 8.

When double-layer films (e.g., Si_3N_4 on SiO_2 on Si) are to be measured, there are four unknowns involved (two layer thicknesses and two refractive index values), so that a single measurement of ψ and Δ cannot provide a complete description. It is possible to treat the two film refractive indexes as known quantities, however, and then relate the measurement to the two layer thick-

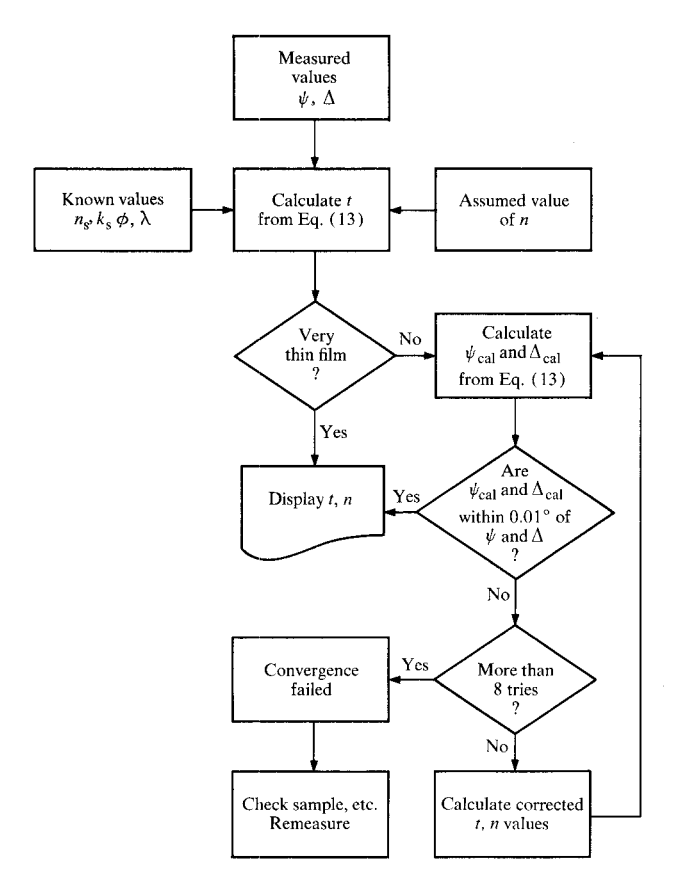


Figure 8 Flow chart of the program in ETA for the numerical inversion of Eq. (13) as indicated in Fig. 1. The inputs are the experimentally determined values of ψ and Δ , the known parameter values and an assumed film refractive index value. The program calculates an initial thickness estimate and then finds correct values of thickness and refractive index or indicates that the iteration procedure did not converge. ETA has a similar program for inverting Eq. (14) for thin double-layer films.

nesses. Calculations by the authors have shown that the error involved in doing this is reasonably small, only a few ångströms, as long as the specified index values are correct in the second decimal place. One can then express the relationship in a form similar to (13),

$$\rho = \tan \psi \, e^{i\Delta} = f(t_{\rm N}, t_{\rm O}, n_{\rm N}, n_{\rm O}, n_{\rm s}, k_{\rm s}, \phi, \lambda), \tag{14}$$

where the subscripts N and O refer respectively to the nitride and oxide layers. Again graphs may be made to show the relationship of the layer thicknesses to ψ and Δ . Curve (c) in Fig. 7 represents a double film with $t_{\rm N}=t_0$ and with total thickness from 0 to 800 Å. Curve (d) represents an 800-Å thick film with varying layer thicknesses. Equation (14) is solved numerically for the layer thicknesses as in the previous case. Here again, initial layer thickness estimates must be provided. ETA accomplishes this by assuming that the film is homogeneous, with refractive index of 1.72 (roughly the aver-

479

age of the two layers); by calculating from (13) an initial thickness estimate; and by assigning half the value to each layer. These initial estimates produce convergence for double layer films with any proportion of oxide and nitride as long as the total film thickness is less than 800 Å.

The programs used by ETA to acquire and analyze the data occupy about 12K 16-bit words of core on an IBM 1130 computer.

Alignment procedure

The alignment procedures for ETA are carried out to insure proper positioning of the light beam and apertures, as well as the proper angles of incidence and component azimuths. The alignment is done once and need not be repeated.

Laser and aperture positioning

The beam-limiting aperture is removed from the light path and the laser vee-block is adjusted with shims in the direct-path mode to aim the beam directly onto the center of the control aperture and to maintain a constant beam height of 6.35 cm (2.50 in.) along both input and detection arms. The limiting aperture is replaced and its support is adjusted with shims to center it on the beam. A temporary alignment aperture is then placed on the detection arm about 40 cm in front of the control aperture and is centered on the beam.

· Angle of incidence verification

With the temporary alignment aperture in place, the arms are raised to the measurement position and a wafer of appropriate thickness is placed on the sample stage. The height of the stage is then adjusted with shims, if necessary, to allow the reflected light to pass directly through both temporary and control apertures on the detection arm. This insures a 70.00° angle of incidence whenever samples of the same thickness as the test wafer are measured. If a sample of different thickness is measured without readjustment of the stage height, the angle of incidence will change during sample alignment by 0.01° for every 0.085 mm (0.0033 in.) difference in thickness. When the sample stage height has been set and fixed, the temporary aperture is removed from the system.

• Alignment of component azimuths

With ETA in the measurement position and the compensator removed, a wafer with an evaporated aluminum film is placed on the sample stage. The analyzer rotation is stopped, and the polarizer and analyzer are manually adjusted to produce a null at the detector. The polarizer is thus positioned in the plane of incidence. This is a precise adjustment, since the PMT voltage may be in-

creased considerably as null is approached. At null the collar on the polarizer mount is engaged in the 0° pinned position and clamped around the polarizer. The PMT voltage is then lowered to its normal range, the analyzer is rotated, and measurements are made of the azimuth of the reflected light. Because the polarizer azimuth is now zero, the reflected light will be linearly polarized in the plane of incidence; thus its azimuth is also zero. The analyzer may be adjusted in its holder until the measured azimuth is zero, or alternatively the value that is actually measured may be entered as an alignment constant in the analysis program and all successive measurements corrected by that amount. This correction is carried out by the application of a rotation matrix corresponding to twice the measured zero azimuth to the vector comprised of the Fourier coefficients. Twice the angle is used since the coefficients of the second harmonic are of interest.

The analyzer is again stopped and the arms lowered to the direct-path configuration. The compensator is first inserted in the incident light path with the fast axis oriented approximately at 90°. The compensator and analyzer are then adjusted for a null at the detector. At null, the detected light is linearly polarized, indicating that the compensator azimuth is precisely at 90°. The collar on the compensator mount is permanently tightened around the compensator. The polarizer, compensator and analyzer are then all correctly aligned with respect to the plane of incidence on the instrument.

The polarizer mount has pinned stops designed to be at 12° and 45° in addition to the 0° alignment position. The angular position of these stops is then measured to within 0.01°. The compensator is removed, the arms are lowered to the direct-path position, and the azimuth of the light coming from the polarizer is measured with the polarizer pinned at these alternate positions. The results are typically found to be within 0.1° of the nominal values. This deviation, however, would produce an unnecessary systematic error in the thickness measurements. Thus in practice the measured polarizer settings are entered into the program and used in the analysis when film measurements are made.

Precision

Random measurement errors are the limiting factor in determining small parameter changes in a measurement. The ability to measure small parameter changes with a high degree of confidence that the observed change is real (and not due to random fluctuation inherent in the measurement) is referred to as the resolution, or precision, of the measurement [9]. We shall use the term precision in this sense and differentiate it from the concept of accuracy, which is discussed in the following section.

The question of precision is an important one in measuring thickness of films in a manufacturing environment, where one is measuring a succession of films that ideally have the same thickness. Here the ability to detect minor deviations in thickness reliably, insofar as they might indicate that a process is beginning to drift while still being within specification, is of obvious value.

The basic parameters that ETA measures are the Fourier coefficients a_2 and b_2 in Eq. (1), which describe the intensity variation of the detected light with the analyzer azimuth. The smallest change in these coefficients that can reliably be measured by ETA is limited by the random fluctuations that appear in repeated measurements of light having constant polarization. To determine the magnitude of these random fluctuations, ETA was placed in the direct-path configuration, and the compensator and the control aperture were removed from the light path. The detected light was thus linearly polarized with an azimuth given by that of the polarizer. The control aperture was removed to avoid the slight influence it appears to have on the polarization of the light in the direct-path configuration, as described below. Then measurements were made of azimuth of the light for a period of over an hour. Each measurement acquired data for ten rotations of the analyzer, a total of 2560 data. The results are shown in Fig. 9, which is a histogram of the number of observations of azimuth values within 0.001° intervals. The overall spread for all readings is 0.012° and the standard deviation of the data is 0.0018°. Similar precision is reported by Scholtens, et al. [10], in an instrument that measures azimuth of nearly linearly polarized light with a rotating analyzer followed by an analog phase detector.

Since the azimuth value is arbitrary in this measurement, we may without loss of generality consider the average value of the readings to be zero. Then from Eq. (3) it follows that for linearly polarized light, where $\chi = 0^{\circ}$, the standard deviation in b_2 is just twice that for α . The same conclusion can be drawn for a_2 from Eq. (2) by considering the azimuth to be 90° . For normal distributions, 95 percent of the values fall within two standard deviations of the average value. Thus, if a change in either a_2 or b_2 equal to four times the standard deviation for α is measured, we have 95 percent confidence that the change was a real one and was not due to random measurement errors. This amount, which we call the measurement uncertainty, is found by converting 0.0018° to radians and multiplying by four, and is given by

$$\delta a_2 \approx \delta b_2 \approx 1.3 \times 10^{-4}. \tag{15}$$

These uncertainties are essentially constant and independent of the polarization of the light arriving at the rotating analyzer. This situation is in contrast to that for conventional ellipsometers, which have a constant un-

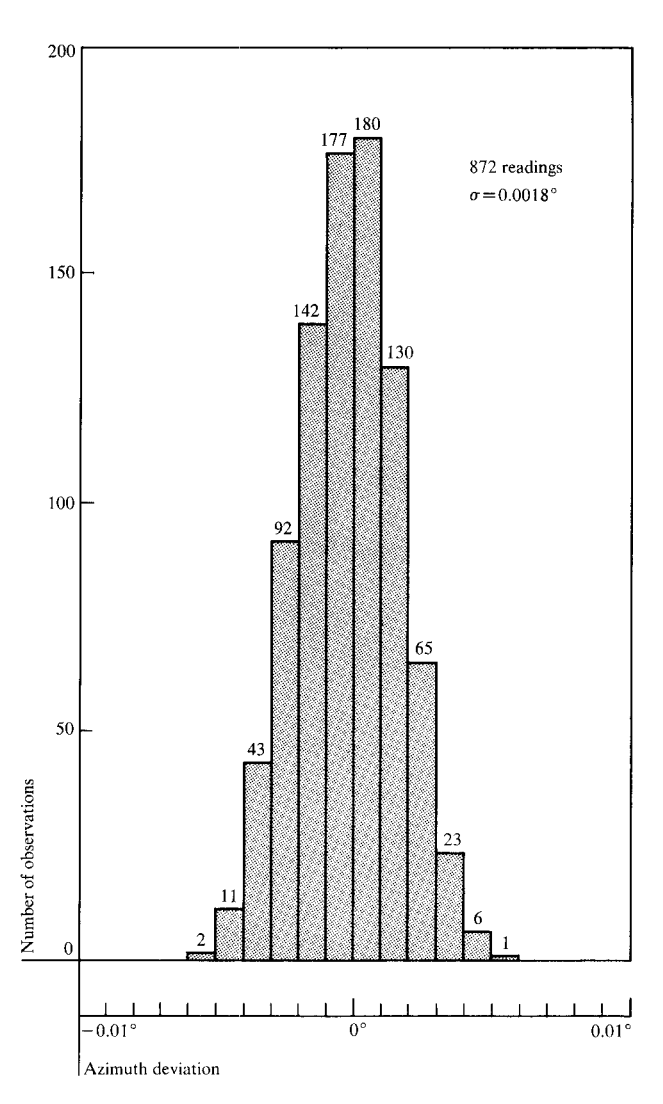


Figure 9 Histogram of observed azimuth readings of linearly polarized light in the direct-path configuration. The total spread is 0.012° and the standard deviation for 872 readings is 0.0018°.

certainty in the ellipsometric sample parameters ψ and Δ of Eq. (7), usually on the order of 0.01°.

The uncertainty associated with measured values of thickness and refractive index can be visualized for a conventional ellipsometer from graphs like that shown in Fig. 7. One simply draws a circle with a radius equal to the uncertainties in ψ and Δ and notes the values of thickness and refractive index that fall within the circle. More quantitatively, the uncertainty in thickness may be determined from Eq. (13).

For each measurement mode of ETA, defined by a relationship of a_2 and b_2 to ψ and Δ , a graph of film thickness and refractive index versus Fourier coefficients can be drawn, analogous to Fig. 7. For the normal measurement mode (i.e., with compensator absent and polarizer

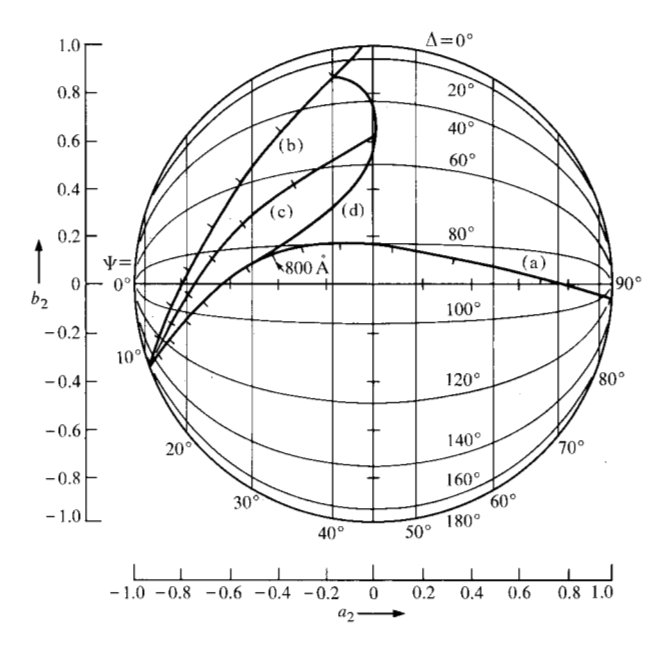
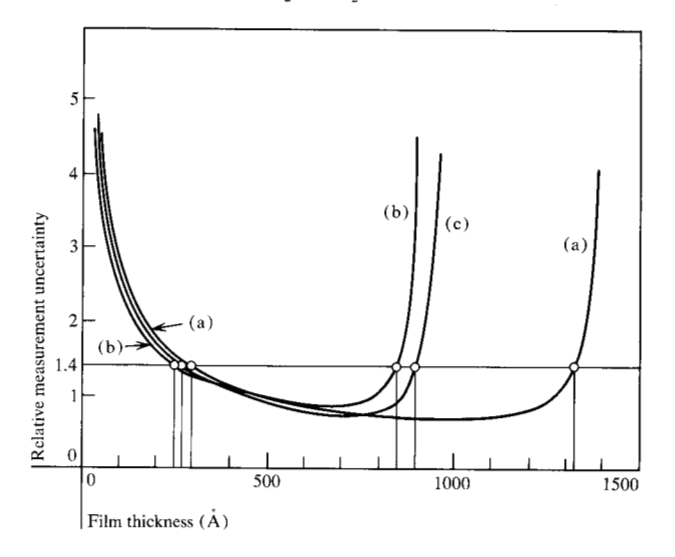


Figure 10 Graph of the Fourier coefficients a_2 and b_2 for the films represented in Fig. 7, with ETA in the normal measurement mode. Lines of constant ψ and Δ are superimposed to show the behavior of Eqs. (4), (5) and (8). Note the extremely reduced variation of the coefficients for films less than 200 Å thick.

Figure 11 The square root of the Jacobian in Eq. (21) plotted vs film thickness for the films represented by curves (a), (b) and (c) in Figs. 7 and 10, for ETA in the normal measurement mode. The vertical axis represents the relative uncertainty in determining ψ and Δ . The value 1.4 makes this uncertainty approximately 0.01° if the uncertainty in determining the normalized Fourier coefficients a_p and b_p is 1.3×10^{-4} .



at 45°), defined by Eqs. (4), (5) and (8), the curves shown in Fig. 7 are transformed as shown in Fig. 10. For comparison, lines of constant ψ and Δ are superimposed. The plot is different from Fig. 7 in that the lines representing $\psi = 0^{\circ}$ and 90° collapse to single points and the entire graph is inverted. Readers familiar with polarimetry may recognize Fig. 10 as a polar view of the Poincaré sphere. If one now draws an imaginary circle representing the measurement uncertanties in a_2 and b_2 it becomes obvious that the range of thickness and refractive index values that fall within the circle varies considerably with position on the graph. The precision with which thickness can be measured by ETA in this measurement mode thus depends on the film thickness. For example, the uncertainty in thickness corresponding to the values given in Eq. (15) is over 2 Å for a 20-Å oxide film, but only 0.12 Å for a 500-Å oxide film. Systematic errors an order of magnitude larger than the random errors would thus make very thin films completely unmeasurable with ETA in this measurement mode. For conventional ellipsometers, assuming 0.01° uncertainty in ψ and 0.02° uncertainty in Δ , the thickness uncertainties are about 0.07 Å and 0.17 Å respectively for 20-Å and 500-Å oxide films on silicon. In the normal measurement mode, ETA is thus more or less precise than a conventional ellipsometer, depending on the thickness of the film being measured.

To make this comparison quantitative, Eqs. (4) and (5) are differentiated with respect to a_2 and b_2 . The Jacobian matrix of partial derivatives is found, using Eqs. (8) for the normal mode, to be

$$\frac{\partial(\psi, \Delta)}{\partial(a_2, b_2)} = \begin{bmatrix} \frac{1}{2}\sin 2\psi & 0\\ (\sin 2\psi \tan 2\psi \tan \Delta)^{-1} (-\sin 2\psi \sin \Delta)^{-1} \end{bmatrix}.$$
(16)

The uncertainties in ψ and Δ with ETA in the normal measurement mode are thus

$$\delta \psi = \delta a_{s}/2 \sin 2\psi, \tag{17}$$

$$\delta \Delta = \delta a_{a}/(\sin 2\psi \tan 2\psi \tan \Delta) - \delta b_{a}/\sin 2\psi \sin \Delta.$$
 (18)

The quantities in (17) and (18) have minimum values for $\psi = 45^{\circ}$, $\Delta = 90^{\circ}$ given by $\delta \psi = \delta a_2/2$, and $\delta \Delta = -\delta b_2$, the values being in radians. Converting to degrees and using (15) give the minimum uncertainties as

$$\delta \psi = 0.0035^{\circ},\tag{19}$$

$$\delta \Delta = 0.007^{\circ}. \tag{20}$$

The determinant J of the matrix in (16) represents a magnification factor for small areas surrounding corresponding points in the (ψ, Δ) plane and the (a_2, b_2) plane [11]. It is given by

 $J = -1/(2 \sin^2 2\psi \sin \Delta). \tag{21}$

The determinant J takes on its minimum value of -1/2 for the same conditions that minimize (17) and (18). (The negative sign is incidental, and merely reflects the fact that Δ and b_2 increase in opposite directions. We subsequently will refer only to its absolute value.) The square root of J can be taken as an estimate of the ratio of short distances, or uncertainties, in the two planes. With this interpretation, it gives a measure of the uncertainty involved in a measurement using ETA relative to that using a conventional ellipsometer. To increase the product of the values in (19) and (20) to $(0.01^{\circ})^2$, J would have to be approximately two, four times its minimum value.

To see how the relative precision of ETA varies with the type and thickness of film being measured, Eq. (21) was evaluated for the values of ψ and Δ assumed for (a), (b) and (c) in Fig. 7. The square root of the result was taken and plotted vs film thickness in Fig. 11. The line at 1.4 shows the approximate thickness limits for precision in measuring ψ and Δ comparable to 0.01°. From the graph for ETA used in the normal mode these limits are 300 to 1300 Å for oxide films [curve (a)], 250 to 850 Å for nitride films [curve (b)], and 300 to 900 Å for composite films of equal layer thicknesses [curve (c)]. These categories typify insulating films appropriate for use in current FET technology.

The precision of ETA is greatly improved for thin films in the thin-film mode (i.e., with polarizer at 12° and compensator at 90°). The effect on ψ_a and Δ_a is described by Eqs. (11). With the assumption, for simplicity, that the compensator is ideal, the point corresponding to zero film thickness is transformed to the point $\psi_a = 45^{\circ}$, or a little less, and $\Delta_a = 90^\circ$, where the precision is greatest. Figure 12 is a plot for ETA in this mode, showing curves for oxide and nitride films. The 0-to-300 Å region, where the change in a_a and b_a is much greater than in the normal configuration mode, is shown for emphasis with solid lines. The portion of the curves for 0 to 200 Å in the normal mode are reproduced for comparison in the lower left part of the circle. In the thin-film mode, an oxide film of 20-Å thickness gives a larger change in a_0 and b_0 than a 200-Å film gives in the normal mode. A plot of relative measurement uncertainty similar to Fig. 11 is shown in Fig. 13 for the thin-film region, again showing the 1.4 line, where precision in ψ and Δ is comparable to 0.01°. Oxide films from 0 to 350 Å and nitride films from 0 to 250 Å fall within this range.

Finally, for films of thickness larger than the values given above, where Δ_a may become greater than 180°, a single measurement in the normal mode does not give enough information to determine the film thickness unambiguously. If the approximate thickness is known, the computer can pick the right answer from the

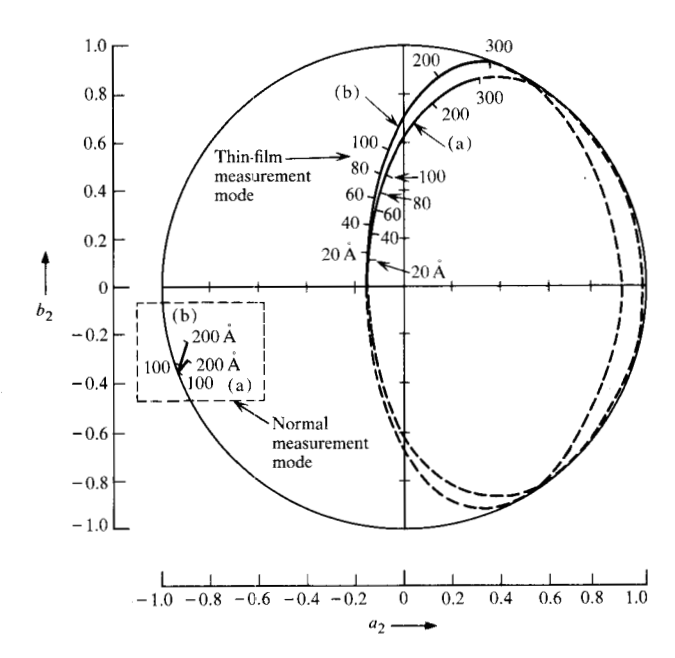


Figure 12 Graph of the Fourier coefficients a_2 and b_2 for the films represented by curves (a) SiO_2 and (b) $\mathrm{Si}_3\mathrm{N}_4$ in Fig. 7, with ETA in the thin-film measurement mode. The full range of thickness values is plotted, with the region of optimum sensitivity (0 to 300 Å) shown as solid lines. The relatively insensitive (0 to 200 Å) region of Fig. 10 is reproduced at the lower left for comparison. The lines of constant ψ and Δ are omitted here for clarity.

Figure 13 Curves of relative uncertainty in determining ψ and Δ vs film thickness for ETA in the thin-film measurement mode. The curves correspond to films represented by curves (a) SiO₂ and (b) Si₃N₄ in Figs. 7 and 10. The line at the value 1.4 has the same meaning as in Fig. 11.

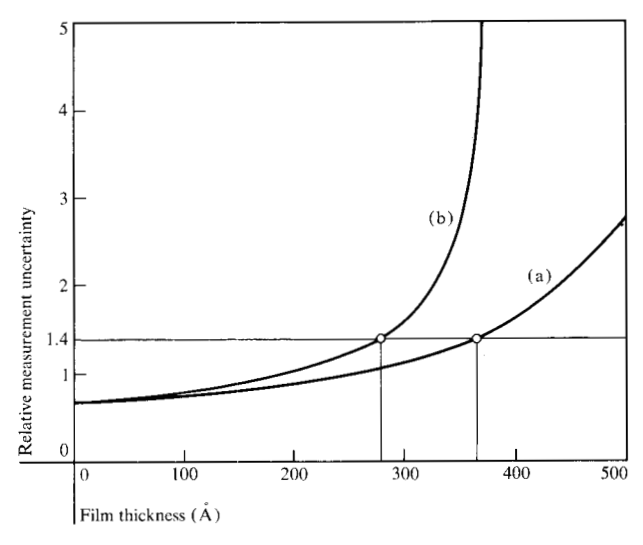


Table 1 Summary of three modes of operation for ETA.

Mode	Polarizer setting	Compensator setting (fast axis)	Type of film	Range of $\Delta_{ m a}$
Normal	45°	Absent	SiO ₂ :300 to 1300 Å Si ₃ N ₄ :250 to 850 Å Double:300 to 900 Å	(0°, 180°
Thin film	12°	90°	SiO ₂ :0 to 350 Å Si ₃ N ₄ :0 to 250 Å	(0°, 180°)
General purpose (two readings)	45°; 45°	Absent; 90°	General use	(0°, 360°)

two mathematically possible ones. Without, this knowledge, however, the normal operation mode may be extended to an "general-purpose" mode by performing a second measurement with the compensator inserted, as described in Appendix 2. This procedure removes the uncertainty for the value of Δ_a mentioned previously.

The three modes of operation described in this section are summarized in Table 1, which lists the settings of the polarizer and compensator, if used, the film type and thickness range for adequate precision, and the range of values taken by Δ_a . It should be noted that in all the configurations described, the only operator adjustments required are switching between two pinned settings for the polarizer and either removing or inserting the compensator. Thus the measurement range of ETA is not limited by its specific design for measuring films in the 300-to-800 Å thickness range without operator adjustment. By including minimal changes in the input optics, very thin films can be measured, e.g., in situ measurements of film growth from a bare substrate, as well as films of arbitrary thickness, all with precision comparable to that of manual ellipsometers.

Accuracy

Systematic measurement errors are the limiting factor in determining the true value of a parameter in a measurement. Even in the presence of large random errors, by numerous repetitions of the measurement and averaging of the results, the true parameter value may be closely determined if systematic errors are negligible. The ability of a measurement to closely determine the true value of the measured parameter is referred to as the accuracy of the measurement [9]. We shall use the term accuracy in this sense, as distinct from precision, as defined in the previous section.

The requirement for accuracy in a measurement is basically that the measurement conform to all the assumptions and parameter values of the theory used to model it and to analyze the data acquired. According to

(13), systematic errors in film thickness and refractive index are a result of systematic errors in the parameter values $(n_s, k_s, \phi, \lambda)$ and in the experimental parameters ψ and Δ . These errors are discussed in this section and an attempt made to quantify them where possible.

The values of n_s and k_s for silicon at 6328 Å are not as precisely known as they are at 5461 Å, where until recently almost all ellipsometric work has been done. The currently used values of 3.855 and 0.024 for n_s and k_s , respectively, were obtained by evaluating a polynomial fit to literature data [8] and may be in error by as much as 0.005 and 0.002, respectively. It is expected that these values will become more accurately determined as further use is made of He-Ne lasers in ellipsometry. The angle of incidence ϕ in ETA is determined by the angular travel of the two arms and by sample alignment. Dimensional tolerances constrain the travel of each arm to be within $\pm 0.003^{\circ}$ of 20° , while sample alignment produces a somewhat larger error, as follows. The control aperture subtends an angle of 0.1° from the point of reflection, so that if the center of the reflected light were only to fall somewhere on the aperture, the angle of incidence could vary by ±0.025° (half the variation of the reflected light). Experience with ETA has shown, however, that the reflected light is centered much better than this, so that the value of $70.00 \pm 0.01^{\circ}$ may be used for ϕ . When samples of more than a few mils difference in thickness are measured, however, the statements in the section entitled "Angle of incidence verification" must be considered.

The experimental parameters ψ and Δ contain systematic errors from a number of sources, most importantly in assumed values of component azimuths, and, for the compensator, ψ_c and Δ_c . Substituting the polarizer azimuth P for 12° in (11) and then differentiating successively with respect to P, ψ_c and Δ_c gives the effect of small errors in these values:

$$\delta\psi = \left(\frac{\sin 2\psi}{\sin 2P}\right)\delta P - \left(\frac{\sin 2\psi}{\sin 2\psi_c}\right)\delta\psi_c,\tag{22}$$

$$\delta \Delta = \delta \Delta_{\rm c},\tag{23}$$

$$\frac{\partial \psi}{\partial \Delta_c} = \frac{\partial \Delta}{\partial P} = \frac{\partial \Delta}{\partial \psi_c} = 0. \tag{24}$$

For the normal measurement mode ($P = 45^{\circ}$, compensator absent) the resulting errors in ψ and Δ are

$$\delta \psi = \sin 2\psi \, \delta P,\tag{25}$$

$$\delta \Delta = 0. \tag{26}$$

For the thin-film measurement mode ($P=12^{\circ}$, compensator present) the errors are somewhat different. Assuming $\psi_c \approx 45^{\circ}$ and the film thickness $\lesssim 300$ Å so that $\psi \lesssim 18^{\circ}$, one obtains

 $\delta \psi \approx \sin 2\psi \ (2.5 \ \delta P - \delta \psi_c)$

$$\lesssim 1.5 \,\delta P - 0.6 \,\delta \psi_{\rm c},\tag{27}$$

$$\delta \Delta = \delta \Delta_c. \tag{28}$$

A constant offset $\delta\theta$ in the azimuth of the rotating analyzer produces an equal error $\delta\alpha$ in the measured azimuth of the polarization ellipse. Its effect on ψ and Δ is found by differentiating (2) – (5) with respect to α , solving for the errors in ψ_a and Δ_a , and then relating them to ψ and Δ . Thus

$$\delta\psi_a = -\cos\Delta_a\,\delta\alpha,\tag{29}$$

$$\delta \Delta_{\rm a} = \left(\frac{2 \sin \Delta_{\rm a}}{\tan 2\psi_{\rm a}}\right) \delta \alpha. \tag{30}$$

These expressions give the errors in ψ and Δ for the normal mode, due to equations (8). Both errors are seen to vanish for circularly polarized reflected light ($\psi_a = 45^\circ$, $\Delta_a = 90^\circ$, 270°), while (30) can become large if ψ_a is close to 0°. This occurs for thin films, and the situation is avoided by switching to the thin-film mode when ψ becomes too small for the normal mode to be used. Then, assuming $\psi \lesssim 18^\circ$ and ψ_a is within 5° of 45°,

$$\delta \psi = \left(\frac{\sin 2\psi}{\sin 2\psi_{\rm a}}\right) \delta \psi_{\rm a} \lesssim -0.6 \cos \Delta_{\rm a} \delta \alpha, \tag{31}$$

$$\delta \Delta = \delta \Delta_{\rm a} \lesssim 0.3 \sin \Delta_{\rm a} \, \delta \alpha. \tag{32}$$

An offset δC in the azimuth of the compensator from its assumed 90° value in the thin-film mode also gives an error in ψ and Δ . Calculations involving a generalized form of equations (11), in which C appears explicitly, give the following expressions, where P has been set to 12° and ψ is assumed $\lesssim 18^{\circ}$:

$$\delta \psi = \left(\frac{\sin 2\psi}{\sin 2P}\right) \delta C \lesssim 1.5 \ \delta C,\tag{33}$$

$$\delta\Delta = \left(\frac{2}{\tan 2P}\right)\delta C \approx 4.5 \,\delta C. \tag{34}$$

A misaligned sample produces an error in the *plane* of incidence as well as in the *angle* of incidence. Since this plane is the common reference for all azimuth values, the resultant error is systematic, although not independent of the other azimuth errors. From geometrical considerations, the sensitivity of the automatic adjustment of the plane of incidence is less than that of the angle of incidence adjustment by a factor of $\sin 20^{\circ}$. The plane of incidence thus carries an approximate $\pm 0.03^{\circ}$ maximum tolerance.

The automatic acquisition of data, which involves the use of amplifiers, an A/D and an angular encoder, provides ETA with high speed and precision, but also may introduce additional systematic errors that are not present in manual ellipsometers. With proper adjustment of offset controls on the A/D and the operational amplifier, and of the PMT supply voltage, however, errors due to offset and nonlinearity can be reduced to negligible levels. Typically, the offset is less than 0.1 percent of the peak signal, and the fourth harmonic (a measure of nonlinearity) is less than 0.2 percent of the average signal level in magnitude. Moreover, when there is not much variation in the light intensity, i.e., when the reflected light is nearly circularly polarized, the residual effects of nonlinearity and offset are greatly reduced

One final source of error was discovered during a series of measurements, similar to those shown in Fig. 9 of the preceding section, which had been made to evaluate the phase stability of the analog circuitry. Over a threeday period, the azimuth of linearly polarized light from a fixed polarizer was measured, with the control aperture present, in the direct-path configuration. The measured azimuth varied slowly between ±0.025° limits, with a period of about two hours, for the entire interval. In light of the extreme stability evident in the data of Fig. 9, taken with the control aperture removed, periodic phase drift of the analog signal cannot be assumed in the interpretation of this data. Although not presently confirmed, it is postulated that slight deviations in the direction of the light coming from the laser occur over a period of time, causing the light to impinge on the control aperture at slightly different locations. If the aperture affects the polarization of the light as it passes through, a continuous variation in azimuth of the amount stated above would not be unreasonable. We are currently investigating this possibility. With proper modification of the aperture, its perturbing effect, if present, should be removed. This effect is presented here as a systematic error since during a measurement, the sample alignment mechanism will tend to keep the light falling on only one portion of the control aperture, making the effect more nearly constant and reproducible. The effect is treated in the following analysis as a systematic analyzer offset.

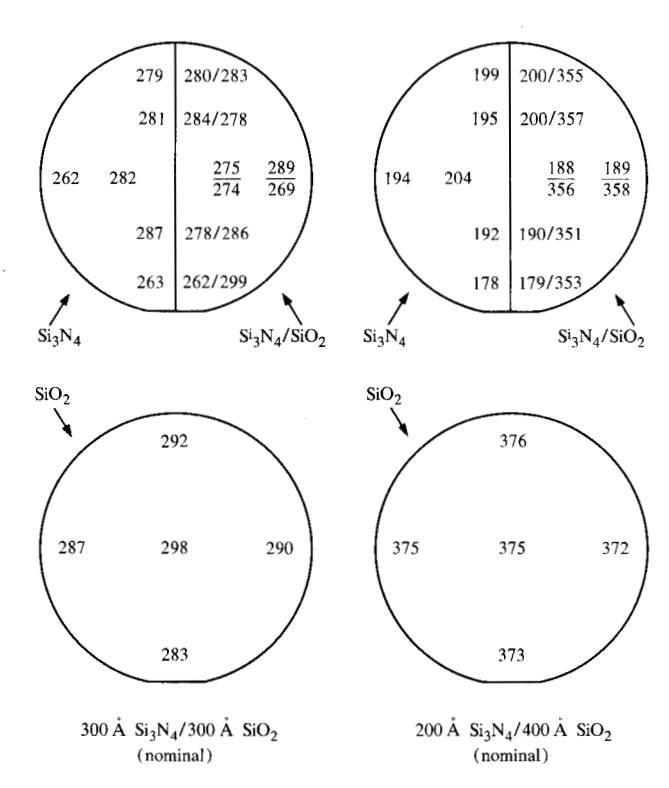


Figure 14 Results of measurement of single- and double-layer films using ETA in the normal measurement mode. The wafers were prepared so that the SiO_2 and Si_3N_4 layer thicknesses could be checked with the single-layer measurements. Regions of nonuniformity in Si_3N_4 thickness are seen to correlate on the two halves of each wafer.

The total effect of errors in component alignment and characterization is seen by combining all the contributions to errors in ψ and Δ given above. For the normal measurement mode, (25), (26), (29) and (30) give

$$\delta \psi = \sin 2\psi \, \delta P - \cos \Delta \, \delta \alpha, \tag{35}$$

$$\delta \Delta = \left\{ \frac{2 \sin \Delta}{\tan 2\psi} \right\} \delta \alpha. \tag{36}$$

For the thin-film mode, (27), (28) and (31)-(34) give

$$\delta \psi \lesssim 1.5 (\delta P + \delta C) - 0.6 (\delta \psi_c + \cos \Delta_a \delta \alpha),$$
 (37)

$$\delta \Delta \lesssim \delta \Delta_{\rm c} + 0.3 \sin \Delta_{\rm a} \delta \alpha + 4.5 \delta C.$$
 (38)

The following estimates of azimuth and parameter errors allow a calculation of worst-case errors in ψ and Δ : $\delta P = \pm 0.02^{\circ}$, $\delta C = \pm 0.01^{\circ}$, (less than δP because the compensator is kept fixed); $\delta \alpha = \pm 0.025^{\circ}$; $\delta \psi_c = \delta \Delta_c = \pm 0.02^{\circ}$. Substituting these values into (35) – (38) with appropriate sign to maximize the total error, we have for the normal mode, assuming $\psi > 18^{\circ}$,

$$\delta \psi \approx \pm 0.05^{\circ},\tag{39}$$

$$\delta \Delta \approx \pm 0.10^{\circ},$$
 (40)

and for the thin-film mode,

$$\delta\psi \approx \pm 0.07^{\circ}$$
, (41)

$$\delta \Delta \approx \pm 0.07^{\circ}$$
. (42)

For oxide films in the 300-to-1300 Å range, (39) and (40) predict thickness errors of 0.2 to 2.0 Å if the refractive index is specified, and 0.4-to-6.0 Å errors if the index is to be determined from the measurement. In the thin-film mode, (41) and (42) predict oxide thickness errors of up to 0.4 Å for a 20-Å film, increasing with film thickness to 1.4 Å for a 300-Å film, with the oxide refractive index specified. These figures reflect only the errors associated with component alignment and characterization, and do not take into account errors in the silicon refractive index values and the angle of incidence. Comparing equations (39) - (42) with (19) - (20) reveals that the systematic errors in ETA can be expected to be approximately an order of magnitude larger than the measurement uncertainty.

Measurement results

Two sets of measurements performed with ETA in the normal measurement mode are described in this section to demonstrate the types of applications described in this paper. First, a set of eight SiO_2 films ranging in thickness from 300 to 1700 Å in steps of about 200 Å were measured with ETA and also with a commercial manual ellipsometer. The results for all films agreed to within 5 Å or better, with a general tendency for the ETA values to be the lower of the two readings. The ETA measurements were repeated several times, giving 1-or-2 Å reproducibility in thickness.

A second set of measurements was made to demonstrate simultaneous determination of layer thicknesses in double-layer (Si₃N₄ on SiO₂) films. Four wafers were prepared in the following manner. Thermal SiO, films were grown on all four wafers (designated A, B, C and D). Wafers A and B were masked over half their areas and the oxide etched away. After the photoresist was stripped, a chemical vapor deposition layer of Si₃N₄ was grown. Wafers A and B thus had double-layer films over half their surfaces and nitride films over the other half. Wafers C and D had oxide films only. Double-layer measurements could thus be made with a means of independently checking the individual layer thicknesses with single-layer measurements. The two pairs of wafers gave a means of determining the uniformity of the film growth process since wafers A and B, as well as C and D, should be identical. Sets of four wafers were prepared in this way for two combinations of layer thicknesses, with $t_{\rm N}/t_{\rm O} = 300$ Å, 300 Å and 200 Å, 400 Å. The results of the measurements for one pair of wafers of each type are shown in Fig. 14.

The nitride films are somewhat less uniform in thickness than are the oxides, and the variation in thickness is at the bottom of both of the wafers shown, on both sides of the boundary. Although there is good agreement between the nitride layer thicknesses in the single- and double-layer measurements, the two determinations of the oxide thickness differ by 15 to 20 Å. The same results were observed in the other pairs of wafers not shown. All measurements were performed twice and values repeated to within 1 to 2 Å. The center portion of each area shown was then measured with a conventional ellipsometer and similar inconsistencies were found. Finally, the nitride film was etched away on the nominally 200 Å, 400 Å wafer so that the underlying oxide film could be measured directly. A series of measurements over the etched area showed the thickness to vary from 352 to 356 Å, in agreement with the findings of the double-layer measurements. During a cleaning step prior to the deposition of the nitride layer, apparently about 20 Å of oxide was inadvertently removed.

To indicate the speed with which one can perform a series of measurements such as this using ETA, we note here that the 68 measurements on the double-layer films, including data analysis and printout of thickness values, took about 20 minutes.

Summary

A fast, highly repeatable and completely automatic ellipsometric measurement system has been described. Film thickness is obtained typically in five seconds. In one mode of operation, single- and double-layer SiO, and Si₃N₄ films from 300 to 800 Å thick can be measured, and SiO, films up to 1300 Å thick; in another mode, very thin films (0 to 300 Å) may be measured. A simple adjustment of the input polarizing optics changes the mode, and for a given mode no operator control or adjustment is required. The mechanical design provides front and rear access to the measurement area at sample height to permit automatic wafer loading and removal, and space is provided to accommodate an electrically driven x-y stage for automatic control of measurement at multiple sites on a wafer. The combination of two measurements allows its use as a general-purpose ellipsometer. Operator skill is required only for initial alignment and calibration, and subsequent checking for proper operation may be made by periodic inspection of the calculated harmonic content of the data, and/or remeasurement of standard test wafers.

One final disclaimer is made here concerning the application of ellipsometry to double-layer films when one of the layers is very thin. Analysis by one of the authors

(P.S.H.) shows that a given measurement error (i.e., in values of ψ and Δ) or an error in assumed layer refractive index values produces an increasingly large absolute error in the deduced value of thickness for the thinner of the two layers when the thickness approaches zero. The percentage error for the thinner layer thus becomes very large. The thicker layer generally remains measurable in any case. As a general guideline, which is supported by these calculations, the restriction should be added that neither layer be less than about 100 Å in thickness if both layer thicknesses are to be accurately determined. (This does not include the case where the thickness and refractive index of one of the layers are accurately known.) The restriction applies even when the layers have comparable thicknesses, which case is analogous to the problem of determining the refractive index of a very thin film.

Up to the present time, ETA has been employed both as an on-line measurement tool in a manufacturing environment and as a general purpose ellipsometer in research studies.

Acknowledgments

The authors gratefully acknowledge the technical assistance of M. L. Phillips in designing and building the computer interface used in ETA, and of J. W. Lee for building the first operating prototype of ETA. Thanks are also due J. L. Mees for the mechanical design of ETA.

Appendix 1: Relationship of Fourier coefficients to polarization parameters

The light falling on the spinning analyzer is described by either of two sets of polarization parameters (α, χ) or (ψ_a, Δ_a) . In the first representation, the electric field is resolved along the major and minor axes of the polarization ellipse. If the major axis, minor axis and direction of propagation form a right-handed coordinate system, the light is described by

$$E_{\text{major}} = \sin (\omega t), \tag{A1}$$

$$E_{\rm minor} = \tan \chi \cos (\omega t). \tag{A2}$$

If angle θ of the transmitting axis of the analyzer and the azimuth α of the major axis are both measured counter-clockwise from the plane of incidence looking toward the source, the transmitted component is simply

$$E_{\theta} = E_{\text{major}} \cos (\theta - \alpha) + E_{\text{minor}} \sin (\theta - \alpha).$$
 (A3)

The intensity $I(\theta)$ of the transmitted light is proportional to $\langle E_{\theta}^2 \rangle$, where the brackets denote a time average over one period of the light. Combining (A1)-(A3), and squaring and averaging give

$$\langle 4E_{\theta}^{2} \rangle = (1 + \tan \chi^{2}) + (1 - \tan \chi^{2}) \cos 2(\theta - \alpha).$$
 (A4)

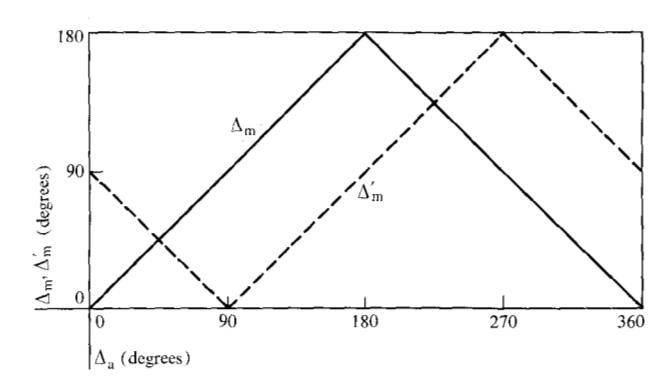


Figure 15 Variation of Δ_m and Δ_m' with Δ_a .

Dividing (A4) by $(1 + \tan^2 \chi)$ gives the normalized intensity

$$I(\theta) = 1 + \cos 2\chi \cos 2\alpha \cos 2\theta$$

$$+\cos 2\chi \sin 2\alpha \sin 2\theta.$$
 (A5)

The normalized Fourier coefficients are thus

$$a_2 = \cos 2\chi \cos 2\alpha, \tag{A6}$$

$$b_2 = \cos 2\chi \sin 2\alpha. \tag{A7}$$

In the second representation, the electric field is resolved along the x and y axes, parallel and perpendicular to the plane of incidence, respectively,

$$E_{x_a} = \tan \psi_a \cos (\omega t + \Delta_a), \tag{A8}$$

$$E_{va} = \cos \omega t. \tag{A9}$$

Now the transmitted component is given by

$$E_{\theta} = E_{x_0} \cos \theta + E_{y_0} \sin \theta. \tag{A10}$$

Combining (A8)-(A10) and squaring and averaging gives

$$\langle 4E_{\theta}^{2} \rangle = (\tan^{2}\psi_{a} + 1) + (\tan^{2}\psi_{a} - 1) \cos 2\theta + 2 \tan\psi_{a} \cos\Delta_{a} \sin 2\theta.$$
 (A11)

Dividing (A11) by $(\tan^2 \psi_a + 1)$ gives the normalized intensity

$$I(\theta) = 1 - \cos 2\psi_a \cos 2\theta + \sin 2\psi_a \cos \Delta_a \sin 2\theta. \tag{A12}$$

The normalized Fourier coefficients are thus

$$a_{2} = -\cos 2\psi_{a},\tag{A13}$$

$$b_{2} = \sin 2\psi_{a} \cos \Delta_{a}. \tag{A14}$$

The inverse relationships for (A6), (A7), (A13) and (A14) are easily seen to be

$$\chi = \frac{1}{2}\cos^{-1}(a_2^2 + b_2^2)^{\frac{1}{2}},\tag{A15}$$

$$\alpha = \frac{1}{2} \tan^{-1} (b_a/a_a), \tag{A16}$$

and

$$\psi_{\rm m} = \frac{1}{2} \cos^{-1} (-a_2), \tag{A17}$$

$$\Delta_{\rm m} = \cos^{-1} \frac{b_2}{\sqrt{1 - a_2}},\tag{A18}$$

where the subscript "m" denotes a parameter determined from a measured quantity. The ranges of values that may be unambiguously determined for these parameters from a single measurement are $(0^{\circ}, 45^{\circ})$ for χ , $(-90^{\circ}, 90^{\circ})$ for α , $(0^{\circ}, 90^{\circ})$ for $\psi_{\rm m}$, and $(0^{\circ}, 180^{\circ})$ for $\Delta_{\rm m}$. To interpret the entire range of azimuth values, the individual signs of a_2 and b_2 in (A6) and (A7) as well as their ratio in (A16) must be considered.

Appendix 2: Removing the ambiguity in the value of $\Delta_{\rm a}$

An ambiguity arises in determining the value for Δ_a when measuring a completely unknown sample, since only $\cos \Delta_a$ is measured. As indicated in Fig. 15, one cannot choose between Δ_m and $360-\Delta_m$ for the correct value of Δ_a . The ambiguity can be removed by performing a second measurement after inserting a quarter-wave plate (QWP) somewhere in the light path with the slow axis in the plane of incidence (x-axis). The effect of the QWP will be to decrease the value of Δ_a by its retardance Δ_c , which is usually very close to 90°. The variation of the new value Δ_{m}' with Δ_{a} is shown in Fig. 15 as a dashed line. One notes that whenever $\Delta_{\rm m} \leq 90^{\circ}$, $\Delta_{\rm a}$ lies in the range (0°, 180°) so that $\Delta_a = \Delta_m$; and $\Delta_m' > 90°$ indicates that Δ_a lies within (180°, 360°), so that Δ_a = $360^{\circ} - \Delta_{m}$. Thus the combination of Δ_{m} values measured before and after insertion of the QWP unambiguously determines the correct value for Δ_a . This is true even if Δ_c is not close to 90°, as long as it is not close to 0° or 180°. The algorithm for determining Δ_a for this more general

$$\Delta_{a} = \begin{cases} \Delta_{m} \\ 360^{\circ} - \Delta_{m} \end{cases} \text{ for } \Delta_{m'} \begin{cases} \leq \\ > \end{cases} \Delta_{c} + \Delta_{m} \left(1 - \Delta_{c} / 90 \right) (B1)$$

References and notes

- F. Reizmann and W. VanGelder, "Optical Thickness Measurement of SiO₂-Si₃N₄ Films on Silicon," Solid State Electronics 10, 625 (1967).
- 2. W. A. Pliskin and E. E. Conrad, "Nondestructive Determination of Thickness and Refractive Index of Transparent Films," *IBM J. Res. Develop.* **8**, 43 (1964).
- 3. Ellipsometry in the Measurement of Surfaces and Thin Films, Eds. E. Passaglia, R. R. Stromberg and J. Kruger (National Bureau of Standards, Misc. Publ. 256, Government Printing Office, Washington, 1964) and Recent Developments in Ellipsometry, Eds. N. M. Bashara, A. B. Buckman and A. C. Hall, North Holland Publishing Company, Amsterdam, 1969.

- K. L. Konnerth and F. H. Dill, "IOTA, A Computer Controlled Thin Film Thickness Measurement Tool," Solid State Electronics 15, 371 (1972).
- 5. For a comprehensive treatment of the spinning analyzer and other polarimetric techniques, as well as the relationship of Fourier coefficients in Eq. (1) to the Stokes parameters, see D. Clarke and J. F. Grainger, *Polarized Light and Optical Measurement*, Pergamon Press, Elmsford, N.Y., 1971, Chs. 1 and 4.
- Chs. 1 and 4.

 6. W. Budde, "Photoelectric Analysis of Polarized Light," Appl. Opt. 1, 201 (1962). In his paper Budde introduces the Fourier analysis of sampled intensity data as a polarimetric technique and demonstrates its inherent precision. The present work automates the procedure, increasing the data acquisition rate by four orders of magnitude, and provides the Fourier analysis immediately upon acquiring the data. The application of the "Fourier-analyzed, spinning analyzer" technique to ellipsometry and the inclusion of the ellipsometric analysis is original with the present work.
- See for example, F. L. McCrackin, E. Passaglia, R. R. Stromberg and H. L. Steinberg, "Measurement of the Thickness and Refractive Index of Very Thin Films and the Optical Properties of Surfaces by Ellipsometry," J. Res. Natl. Bur. Stand. 67A, 363 (1963).

- H. R. Philipp and E. A. Taft, "Optical Constants of Silicon in the Region 1 to 10 ey," *Physical Review* 120, No. 1, 37 (1960), and W. C. Dash and R. Newman, "Intrinsic Optical Absorption in Single-Crystal Germanium and Silicon at 77°K and 300°K," *Physical Review* 99, No. 4, 1151 (1955).
- N. H. Cook and E. Rabinowicz, Physical Measurement and Analysis, Addison-Wesley Publishing Co., Inc. Reading, Mass., 1963, pp. 44-48.
- D. J. Scholtens, J. F. Kleibeuker, and J. Kommandeur, "Apparatus for the Measurement of Magneto-Optical Rotation and Ellipticity," Rev. Sci. Instrum. 44, No. 2, 153 (1973).
- See, for example, Mathematics of Physics and Modern Engineering, I. Sokolnikoff and R. Redheffer, McGraw-Hill Book Co., Inc. New York, 1958, p. 273.

Received April 26, 1973

The authors are located at the IBM Thomas J. Watson Research Center, Yorktown Heights, New York 10598.